Highly carbon resistant multicore-shell catalyst derived from Ni-Mg phyllosilicate nanotubes@silica for dry reforming of methane

Zhoufeng Bian, Ivan Yulian Suryawinata, Sibudjing Kawi *

Department of Chemical and Biomolecular Engineering, National University of Singapore, Singapore 117585, Republic of Singapore

ABSTRACT

Dry reforming of methane (DRM) has been a popular research topic since it consumes two kinds of so-called "green gas" and produces syngas (mixture of CO and H_2) which is commonly used as fuel or feedstocks for chemical industry. In this report, we describe a multicore-shell catalyst derived from Ni-Mg phyllosilicate nanotubes@silica and test it for DRM. After Ni-Mg phyllosilicate nanotubes (PSNTS) were synthesized, a layer of mesoporous silica with a thickness of ~10 nm was coated by a modified Stöber method of hydrolysis of tetraethyl orthosilicate (TEOS) in an ethanol solution mixed with ammonia and cetrimonium bromide (CTAB). After coating, the thermal stability was significantly improved. Upon reduction by H_2 at high temperature, multiple small Ni particles were observed to be supported along the nanotube as well as encapsulated by silica shell. When tested for dry reforming of methane, this multicore-shell catalyst showed a high and stable conversion during a 72 h durability run at 750 °C and much improved carbon resistance than uncoated sample which decomposed at such a high temperature. Due to its high thermal stability and excellent carbon resistance, it is believed that this catalyst can be used for other high temperature and high carbon coking reaction such as biomass gasification.

© 2016 Elsevier B.V. All rights reserved.
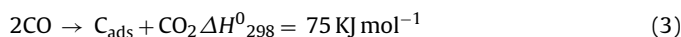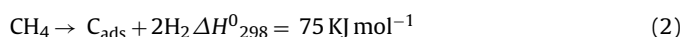
1. Introduction

It is well known that fossil fuel is the main energy source and the vast utilization of fossil fuel comes with two crucial problems: one is the depletion of fossil fuel while the demanding for energy keeps increasing requesting a need to investigate new available resources like natural gas. The other is global warming issue caused by huge amount of CO_2 produced and released into atmosphere [1]. The reaction of CO_2 and methane is considered as one of the important and attracting topics in catalysis, energy and environment research field because it reduces and recycles the greenhouse gases meanwhile produces syngas (mixture of CO and H_2) which is commonly used as fuel or feedstocks for chemical industry [2–4].

DRM is a highly endothermic reaction shown in Eq. (1):

$$CO_2 + CH_4 \rightleftharpoons 2H_2 + 2CO \, \Delta H^0_{298} = 247 \, KJ \, mol^{-1} \quad (1)$$
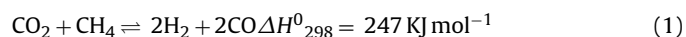
Considering the high reaction temperature (700∼900 °C), highly thermal stable catalysts are required to meet the industrial requirement. Due to the low cost and wide availability, Ni-based catalysts are more practical for industrial utilization [5]. However, Ni-based catalysts always suffer from severe carbon deposition, and the main reason that causes the deactivation of catalysts, which

originates from methane cracking Eq. (2) and Boudouard reaction Eq. (3):

$$CH_4 \rightarrow C_{ads} + 2H_2 \, \Delta H^0_{298} = 75 \, KJ \, mol^{-1} \quad (2)$$

$$2CO \rightarrow C_{ads} + CO_2 \, \Delta H^0_{298} = 75 \, KJ \, mol^{-1} \quad (3)$$

Hence, it is crucial to develop catalysts which can inhibit carbon deposition effectively and a lot of effort has been made to achieve this target. It is well acknowledged that prevention of sintering of Ni particles can help to resist carbon formation in that it can suppress the methane cracking reaction [6–8]. Several methods have already been demonstrated to be feasible to enhance the carbon resistance: promoters [9–12], effect of preparation method [13–15], synergic effect of alloy [16–18], formation of spinel [19] and perovskite structure [20–22]. Recently core-shell catalysts especially metal@silica have been investigated a lot due to its unique structure which can efficiently inhibit sintering of active metal and prevent carbon deposition [23–26]. Li et al. synthesized Nil@silica core-shell and yolk-shell, as well as Ni@Ni-Mg phylloslicate catalysts, presenting superb stability and excellent carbon resistance for DRM [27–29]. Commonly, nickel nanoparticles were synthesized with hydrothermal method, followed by a coating step where tetraethyl orthosilicate (TEOS) hydrolyzed to form a layer of silica enclosing those nanoparticles. Similarly, Ni@alumina [30], Ni@TiO_2 [31] and Ni@ZrO_2 [32] were also synthesized with this route and showed good catalytic performance and carbon resistance.
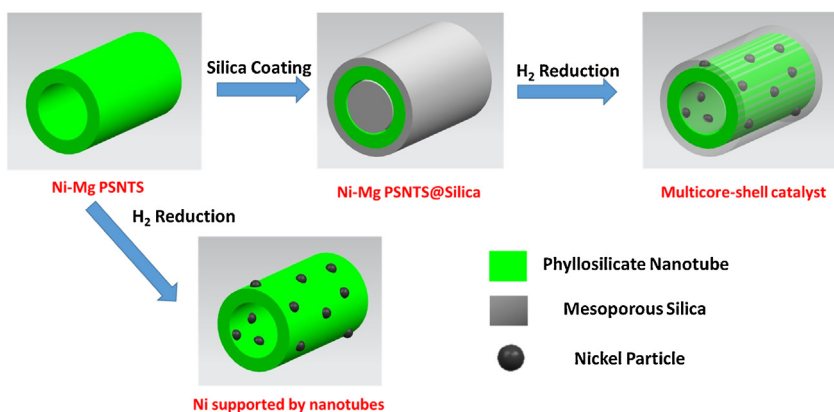
Scheme 1. Scheme of preparation of multicore-shell catalyst derived from Ni-Mg PSNTS@silica.

However, this route is quite tedious and unavoidably some shells may contain multiple nickel cores while some nickel cores may not be encapsulated, both of which may lead to metal sintering. Therefore, now researchers start to design and investigate catalysts of other nano-morphology conferring the confinement effect similar with core-shell structure [33]. In Zeng's review, it is suggested to integrate active nanostructured catalysts with boundary-defined catalyst supports that are "not-so-nano" in dimension to keep the essence of traditional "catalyst-plus-support" type as well as the advantages of nanoscale engineering [34]. Zhang et al. used integrated Ni phyllosilicate nanotubular core-sheath catalysts and claimed its confinement effect helped to suppress carbon formation in the reaction of steam reforming of ethanol [35].

Another practical way could be making multicore-shell catalysts by taking carriers already supporting multiple metal nanoparticles or containing their precursors as the core instead of single metal nanoparticles. Thus, the metal nanoparticles are not only encapsulated but also supported, which can help to avoid the sintering issue which may occur for traditional core-shell catalysts. Han et al. deposited as-prepared Ni nanoparticles onto silica nanospheres, followed by silica coating afterwards. This catalyst showed high carbon resistance with minimal sintering for DRM [36]. Du et al. took NiMgAl-double layer hydroxide (LDH) nanoplates as the core and managed to coat a layer of mesoporous silica encapsulating LDH nanoplates for DRM exhibiting good carbon resistance as well [37].

Herein, we report design and synthesis of multicore-shell catalyst derived from Ni-Mg PSNTS@silica for dry reforming of methane as shown in Scheme 1. Ni-Mg phyllosilicate nanotubes as nickel carriers, were chosen to be cores. Then a layer of mesoporous silica was coated successfully which was characterized with TEM, XRD and BET. After reduction by H_2 at high temperature, multiple uniform Ni particles of small size were observed to be supported along an individual nanotube as well as encapsulated by a single silica shell. This multicore-shell catalyst showed much improved thermal stability compared with the uncoated Ni-Mg PSNTS which would decompose at 750 °C. It also demonstrated good stable activity and excellent carbon resistance in a 72 h durability test at 750 °C, which was attributed to the confinement effect as well as interaction between metal and nanotubular support conferred by the unique multicore-shell structure.

2. Experimental conditions

2.1. Catalysts preparation

All the chemicals were purchased from Sigma-Aldrich Company (Singapore) without any treatment before use. Ni-Mg PSNTS were synthesized by hydrothermal method. Typically, 1.2 g

$Mg(NO_3)_2 \cdot 6H_2O$ and 1.1 g $Ni(NO_3)_2 \cdot 6H_2O$ were dissolved in a mixture of 30 ml DI water and 90 ml ethanol. 2.4 ml sodium silicate solution was then added. After 10 min stirring, 3.0 g NaOH pellets were added and stirred for another 30 min. The dispersion was sealed in an autoclave, heated to 190 °C and maintained at this temperature for 48 h. The obtained emulsion was centrifuged to get green precipitate which was washed with ethanol twice to remove the remaining ions and finally dried at 60 °C in vacuum. The solid was milled into powder and calcined at 650 °C for 4 h.

100 mg as-prepared Ni-Mg PSNTS was dissolved in a mixture of 30 ml DI water and 90 ml ethanol. 0.4 g CTAB was added in the solution was treated by sonication for 2 h to get a clear emulsion. 3 ml ammonia (25%) was put in. Then 0.2 ml TEOS as silica source dissolved in 40 ml ethanol was added drop wise into the solution which kept stirring. The emulsion was at last centrifuged and washed with ethanol twice. After dried, the solid was milled into powder and calcined at 450 °C for 30 min followed by 750 °C for 4 h to removal CTAB and other remaining organic species.

2.2. Catalyst characterization

JEOL TEM was employed to characterize to morphology of fresh, reduced and spent catalysts. Typically corresponding powders were put into ethanol, treated with sonication for several minutes and dropped onto copper grids.

XRD patterns were obtained by Bruker D8 Advance X-ray diffractometer using a Cu Kα radiation ($\lambda = 0.154056$ nm) with acceleration voltage of 40 kV and beam current of 30 mA.

N_2 adsorption–desorption isotherm experiments were performed at 77 K with Micromeritics ASAP 2020 – Physisorption Analyser. Before analysis, the samples were degassed in vacuum at 350 °C for 4 h. The surface area was calculated using BET method and pore volume was obtained with BJH method.

Ni loading was measured with Thermal Scientific iCAP 6000 ICP-OES Analyser. 10 mg powder was dissolved in a mixture of 0.5 ml HF (48%), 2 ml HNO_3 (60%) and 2 ml H_2O_2 aided by ultrasonic treatment and finally diluted with DI water into a total volume of 40 ml. Ni, Mg and Si solutions with known concentration were prepared as calibration standards as well.

H_2-TPR was performed on Thermal Scientific TPDRO 1100 apparatus equipped with a thermal conductivity detector (TCD). Typically, 20 mg sample was tested with a flow of 5% hydrogen in nitrogen (30 ml/min) with a temperature ramping rate of 10 °C/min after degassing with helium for 10 min.

The metal dispersion measurement was carried out on Thermal Scientific TPDRO 1100 as well with N_2O decomposition method reported elsewhere [38,39]. 50 mg sample was reduced at 650 °C by 5% hydrogen in nitrogen for 1 h, and cooled down to 80 °C at the
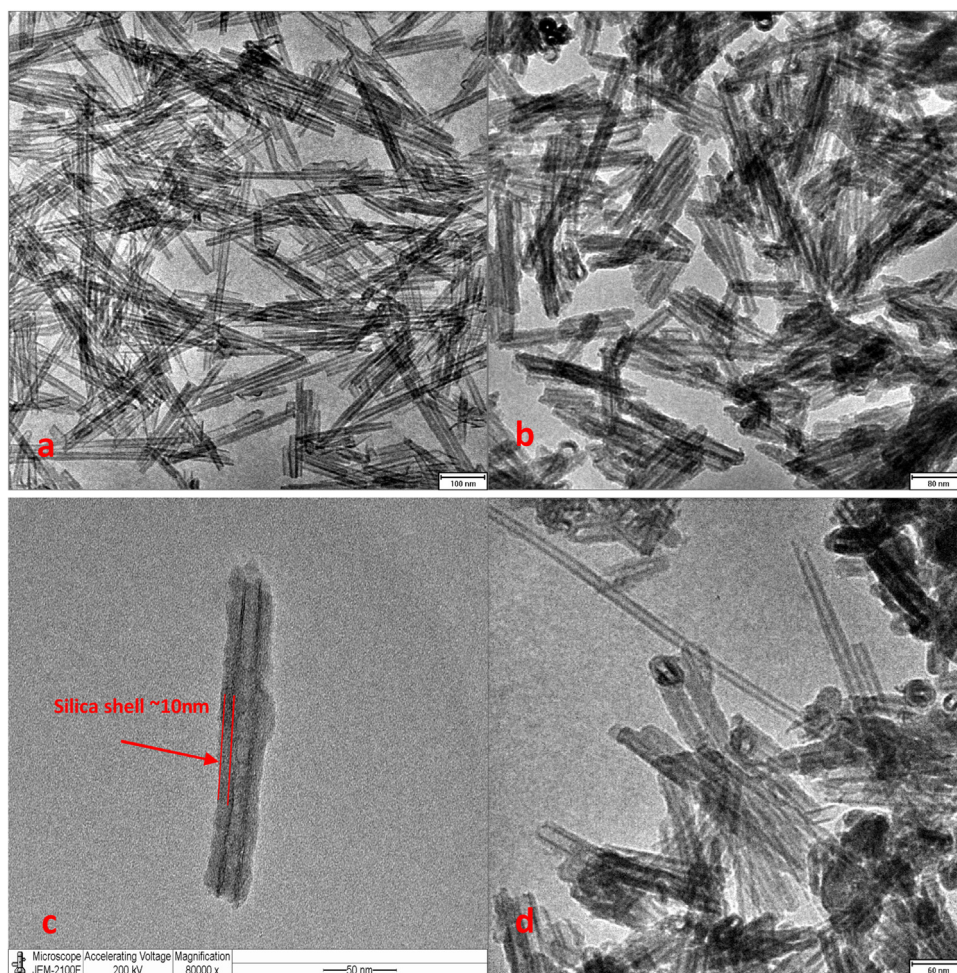
Fig. 1. (a) TEM image of fresh Ni-Mg PSNTS. (b) and (c) TEM image of as-prepared Ni-Mg PSNTS@silica. (d) TEM image of coated Ni-Mg PSNTS without assistance of CTAB.
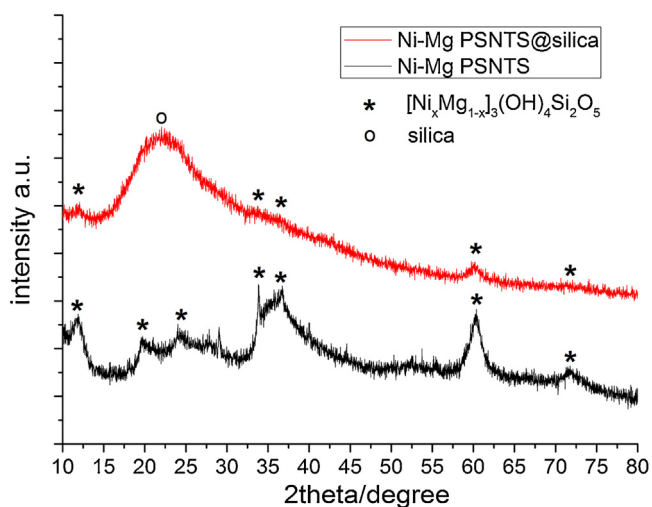

Fig. 2. XRD patterns of fresh Ni-Mg PSNTS and Ni-Mg PSNTS@silica.

atmosphere of nitrogen. Purified N_2O pulses were injected until the eluted peak area was constant. Then the sample was reduced again in a TPR process. The metal dispersion was estimated by comparing the amount of H_2 consumed in first and second TPR process, according to Eqs. (4) and (5).

$$Ni_{Surface} + N_2O \rightarrow NiO + N_2 \tag{4}$$

$$NiO + H_2 \rightarrow Ni + H_2O \tag{5}$$

TGA was carried out on a thermogravimetric analyzer (Shimadzu DTG-60) in static air. The weight was monitored when the temperature went up from room temperature to 800 °C at a rate of 10 °C/min.

2.3. Catalytic DRM reaction

DRM reaction experiments were conducted in a quartz tube reactor whose inner diameter of 4 mm under atmospheric pressure. Before test, catalyst was milled and particle size was made smaller than 125 μm with a sieve. 30 mg catalyst was weighted and put into the tube in the middle of two quartz wood. Before reaction, the catalyst was reduced by pure H_2 (30 ml/min) at 650 °C for 1 h. Helium was flushing then. After the temperature rised to the set reaction temperature (750 °C), the reactants CO_2 and CH_4 were introduced with helium as a carrier gas. The flow rate of all three gases was set to be 10 ml/min controlled by mass flow controllers. The flow rate of outlet gas was measured by a bubble flow-rate meter. The composition of outlet gas was analysed online by a gas chromatograph (Agilent 7820A) equipped with a thermal conductivity detector (TCD).

CO_2 and CH_4 conversion was calculated by following equations:

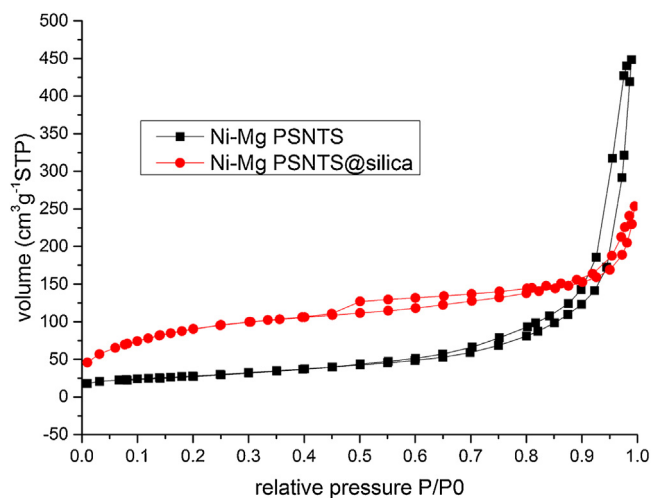$$CO_2 Conversion = \frac{CO2 flowrate_{in} - CO2 flowrate_{out}}{CO2 flowrate_{in}} \tag{6}$$

Fig. 3. N2 isotherms of Ni-Mg PSNTS and Ni-Mg PSNTS@silica.

$$CH_4 Conversion = \frac{CH4flowrate_{in} - CH4flowrate_{out}}{CH4flowrate_{in}} \quad (7)$$

The carbon balance was ±5% for all catalytic runs.

3. Results and discussion

3.1. Characterization of fresh catalysts

TEM was done to confirm the formation of nanotubes as well as the silica shell. As we can see from Fig. 1(a), highly pure nanotubes with uniform diameter were obtained by hydrothermal method as described in our previous work [40]. Silica coating was carried out by a modified Stöber method in which TEOS acts as silica source and CTAB as surfactant and structure-directing agent [41]. As displayed in Fig. 1(b) and (c), a layer of silica in a thickness of ~10 nm formed along and enclosing the nanotubes and the inner pore of nanotubes was as well filled by silica. Without the assistance of CTAB in the synthesis process, the coating was not uniform and many nanotubes were still naked (Fig. 1(d)).

XRD was conducted to confirm the formation of silica shell as well. In Fig. 2, Ni-Mg PSNTS show typical peaks for phyllosilicate species (11.8°, 19.7°, 24.2°, 34.7°,36.5° and 59.8°), indexed to JCPDS#43-0584 ($[Ni_xMg_{1-x}]_3(OH)_4Si_2O_5$) [42]. After coating, typical phyllosilicate peaks are still observable and a broad peak around 22° appears which could be assigned to the silica shell.

The textural properties of these two samples were characterized by N_2 isothermal adsorption-desorption method and displayed in Fig. 3 and Table 1. Both Ni-Mg PSNTS and Ni-Mg PSNTS@silica showed a Type H1 hysteresis indicating the presence of mesopores. However, from Table 1 we can see Ni-Mg PSNTS@silica holds a much higher surface area than uncoated sample. However, its pore volume is significantly lower than that of uncoated Ni-Mg PSNTS. The surface area of uncoated Ni-Mg PSNTS mainly comes from the hollow structure of nanotubes. After coating, mesoporous silica not only covers the outer surface but also fills the inner pore of nanotubes, decreasing the pore volume undoubtedly. However, since the silica shell is mesoporous where a lot of small pores contribute to surface area, a three-time larger surface area is achieved. This is indicated by the much smaller pore size as well. Besides, due to the increase of mass of silica, Ni loading drops from 18.8% to 11.6%.

H_2-TPR was performed and results were plotted in Fig. 4. Ni-Mg PSNTS are constructed by Ni/MgO(OH) and silica nanosheets overlapping with several layers [43]. Ni-Mg PSNTS exhibits two peaks: the first peak appearing at 688 °C is thought to be the reduction
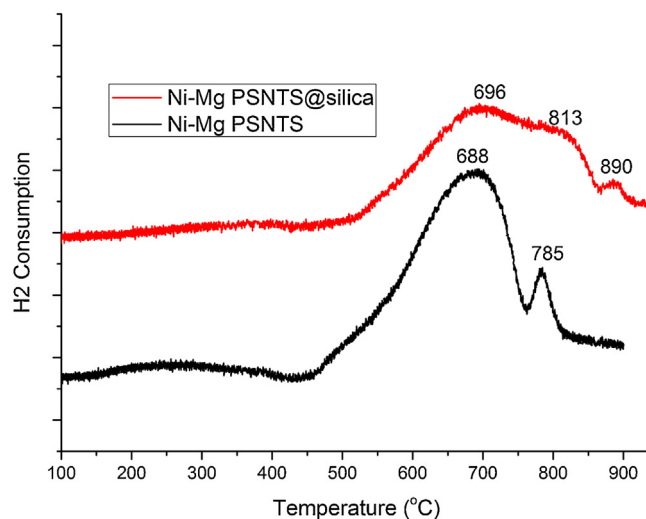

Fig. 4. H_2-TPR profiles for Ni-Mg PSNTS and Ni-Mg PSNTS@silica.

of Ni^{2+} ions located on the outer and inner surface of nanotubes while Ni^{2+} ions incorporated in bulk phyllosilicate nanotubular structure needs a higher reduction temperature depending on the crystallinity [35]. After coating, the main reduction peaks shifts to higher temperature and become broader, and an extra peak occurs at 890 °C. It is proposed that the interaction between NiO and silica for core-shell catalysts can increase the reduction temperature [26,44]. First peak is assigned to Ni^{2+} species weakly interacting with silica while the second peak around 813 °C belongs to those forming a strong interaction with silica. The last peak is still reduction of Ni^{2+} ions incorporated in bulk phyllosilicate nanotubular structure which now needs a higher temperature probably due to the barrier effect of silica shell.

3.2. Characterization of reduced catalysts

TEM was done for reduced catalysts to investigate the morphology and estimate Ni particle size distribution. Fig. 5(c) and (d) displayed reduced Ni-Mg PSNTS. It can be seen that Ni particles with a mean diameter of 10 nm were attached to both inner and outer surface of nanotubes. Reduced Ni-Mg PSNTS@silica were presented in Fig. 5(a): Ni nanoparticles with a mean diameter of 8.5 nm were uniformly dispersed and supported along the nanotubes as well as enclosed by the silica shell, forming a multicore-shell catalysts as shown in Fig. 5(b).

Noticeably, although reduced Ni-Mg PSNTS@silica had a smaller Ni particle size, its metal dispersion (shown in Table.1) measured by N_2O decomposition was even lower than that of reduced Ni-Mg PSNTS. It was reported that typically for Pt@ceria core-shell catalysts, as most of the metal is actually encapsulated such that virtually less metal surface would be exposed for CO chemisorption leading to a much lower active surface area than expectation based on particle size [45]. Similarly coverage of silica shell might inhibit N_2O decomposition resulting in such a discrepancy here.

3.3. Catalytic performance of catalysts

DRM at 750 °C was conducted to examine the catalytic performance for both Ni-Mg PSNTS and Ni-Mg PSNTS@silica. As can be seen in Fig. 6, Ni-Mg PSNTS@silica exhibited a high conversion of CO_2 (89%) and CH_4 (85%) with H_2/CO ratio of 0.8 and kept stable in a 72 h run, indicating its excellent activity and stability for DRM.

Table 1
Chemical-physical properties of Ni-Mg PSNTS and Ni-Mg PSNTS@silica.

sample	surface area[a] m²g⁻¹	Pore volume[a] cm³g⁻¹	Pore size[a]nm	Element ratio[b] wt.%			Dispersion[c]
				Ni	Mg	Si	
PSNTS	100.1	0.69	27.3	18.8	15.1	25.6	6.6%
PSNTS@silica	315.8	0.34	5.0	11.6	9.2	33.6	3.0%

[a] Measured by N_2 isothermal adsorption-desorption.
[b] Element ratio measured by ICP-OES.
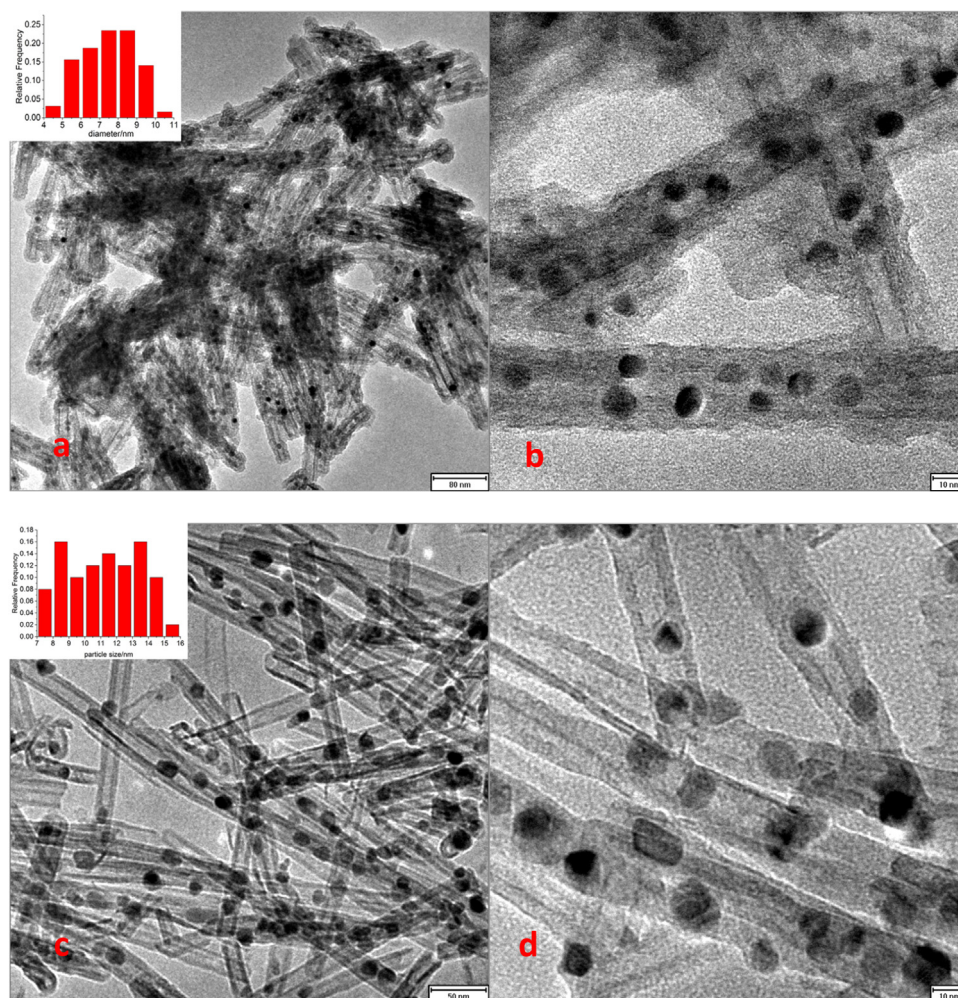[c] Nickel metal dispersion determined by N_2O decomposition.

Fig. 5. (a) and (b)TEM image of Ni-Mg PSNTS@silica reduced by pure H_2 at 650 °C for 1 h, inset is the particle size distribution. (c) and (d) TEM image of Ni-Mg PSNTS reduced by pure H_2 at 650 °C for 1 h, inset is the particle size distribution.

It is commonly acknowledged that due to the existence of reverse water-gas shift (RWGS) in Eq. (8):

$$CO_2 + H_2 \rightleftharpoons H_2O + CO \Delta H^0_{298} = 41.1 \, KJ\,mol^{-1} \qquad (8)$$
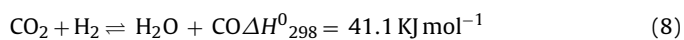
CO_2 conversion is usually higher than methane conversion and H_2/CO would be less than 1 as well. On the other hand, although the initial conversion was similar with Ni-Mg PSNTS@silica, uncoated Ni-Mg PSNTS showed a continuous dropping conversion for both CO_2 and methane. And H_2/CO ratio kept decreasing simultaneously. After a 38 h run, the reactor was blocked, caused by heavy carbon formation.

3.4. Characterization of spent catalysts

TEM was conducted for spent catalysts to investigate their morphology after reaction. It could be seen in Fig. 7(a) that after Ni-Mg PSNTS@silica experiencing a time of 72 h on stream at 750 °C, Ni particles grew a bit larger to a mean diameter of 10 nm, but no obvious metal sintering was observed. Although there were multiple metal particles within one shell, severe sintering was avoided since they were supported by nanotubes. And the multicore-shell structure was well reserved with no significant carbon formation observed. While for the sample of spent uncoated Ni-Mg PSNTS, there was no longer nanotubular structure observed in Fig. 7(b). Instead, Ni particles with bulky silica could be seen with significant formation of carbon nanotubes. It was reported that Ni-Mg PSNTS was not highly thermal stable and would decompose at 680–700 °C
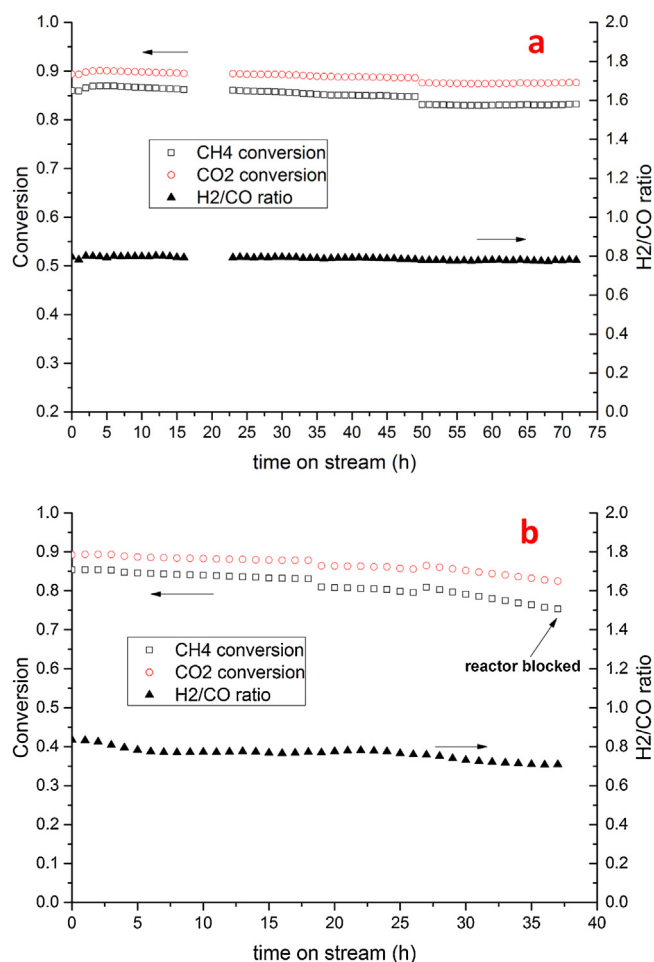
Fig. 6. Catalytic performance of (a) Ni-Mg PSNTS@silica and (b) Ni-Mg PSNTS during a stability test for DRM at 750 °C including CO_2, CH_4 conversion and H_2/CO ratio. (Catalyst amount was 30 mg. Flow rate: CO_2 = CH_4 = He = 10 ml/min. i.e. 33.3% CO_2, 33.3% CH_4, 33.3% helium with a total flow rate of 30 ml/min. GHSV = 60Lgcata^{-1} h^{-1}.)

[46]. Actually, in our primary study where Ni-Mg PSNTS was calcined at 750 °C for 4 h, nanotubular structure collapsed and bulky silica formed (Fig. S1). Thus it was not surprised that uncoated Ni-Mg PSNTS decomposed in a DRM test at 750 °C and those Ni particles losing supports generated much carbon during the reac-

tion. The improvement of thermal stability may be explained: After coating, silica is supposed to form a strong interaction with inner and outer surface of phyllosilicate nanotubes. In other words, phyllosilicate nanotubes are "sandwiched" by inner and outer layers of silica, making the phyllosilicate structure less determinant to deform under high temperature, hindering the structural internal failure. Similar observation was reported: Pt@silica can preserve its morphology after calcination even at 750 °C though bare Pt nanoparticles easily deform and sinter above 300 °C [47].

In order to show the high thermal stability of silica shell, we did calcination for Ni-Mg PSNTS@silica at 800 °C for 4 h, the morphology of silica shell was still well-kept, as shown in Fig. S2. In a brief conclusion, dense and highly thermal stable silica shell protects Ni-Mg phyllosilicate nanotubular core from deforming and decomposing.

TGA was employed to further study carbon formation for spent catalysts and the results are shown in Fig. 8. Up to 800 °C, spent Ni-Mg PSNTS@silica did not show significant weight loss and there was no sharp peak along the DTA curve, indicating there was almost no carbon formation for this sample. On the other hand, spent Ni-Mg PSNTS exhibited a 45% weight loss at 450–650 °C; correspondingly its DTA curve showed a sharp positive peak at 590 °C implying the combustion of deposited carbon [48], both indicating a severe carbon deposition of this catalyst. As a result, TGA curves were quite consistent with what was shown in TEM images.

Confinement effect has been come up to refer to modifications of catalytic properties derived from confined space in encapsulating structures [33,49]. Though metal nanoparticles are not entirely encapsulated with the wall of nanotube-type support, core@tube structure still can help to prevent metal nanoparticles from agglomeration thus supressing carbon deposition and improving catalysis stability [50]. However, in our work, due to the high reaction temperature, Ni-Mg PSNTS cannot maintain its nanotubular structure any more. Therefore, naked Ni-Mg PSNTS did not give a satisfactory performance and heavy carbon deposition occurred. After coating, inert silica shell known to be highly thermal stable, improved the thermal stability, preventing it from decomposing at a temperature as high as 750 °C.

Further, in Du et al. work mentioned previously, nickel being incorporated in mixed oxide nanoplates (NiMgAl-LDH) was regarded as first confinement and coating with mesoporous silica shell was seen as second confinement. It was testified that this unique dual confinement structure of NiMgAl-LDH@silica showed good carbon resistance and high catalytic stability for DRM [37]. Similarly, after reduction, uniformly-distributing nickel nanopar-
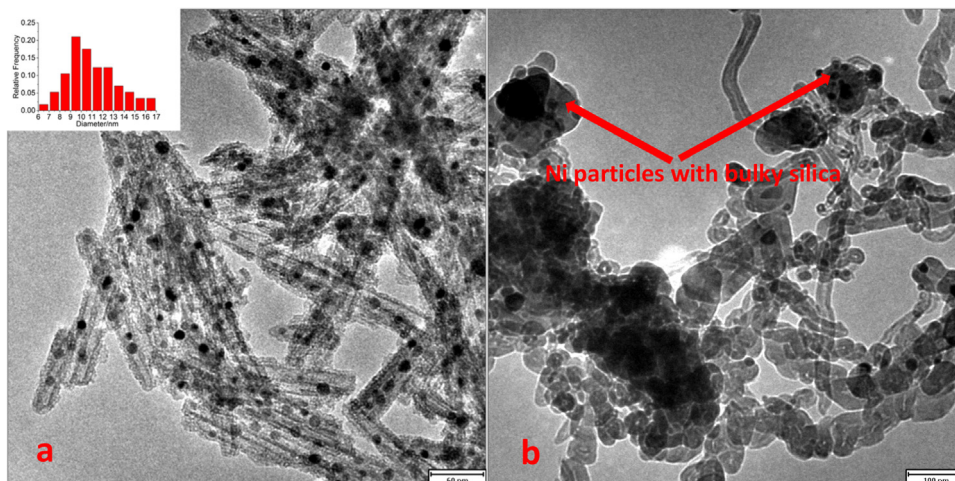

Fig. 7. (a) TEM image of spent Ni-Mg PSNTS@silica after 72 h stability test, inset is the particle size distribution. (b) TEM image of spent Ni-Mg PSNTS after 38 h stability test.
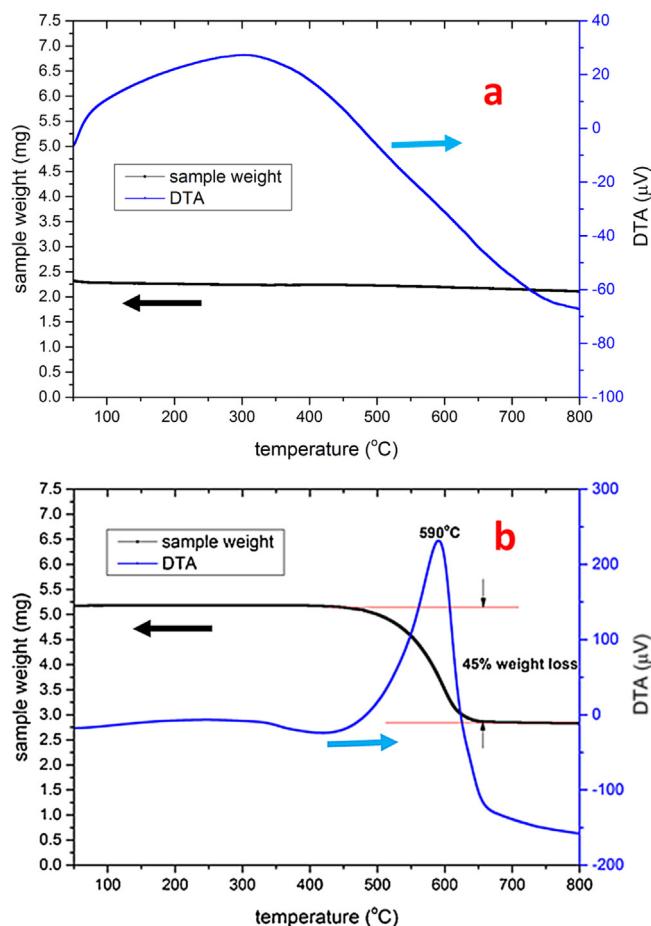
Fig. 8. TGA profiles for (a) spent Ni-Mg PSNTS@silica and (b) spent Ni-Mg PSNTS.

ticles were interacted with and partially encapsulated by the wall of phyllosilicate nanotubes, providing a core@tube confinement. While the mesoporous silica shell actually served as second confinement. Such a dual confinement effect is responsible for its superb carbon resistance and high catalytic stability.

Finally, it can be concluded that coating of silica not only improved thermal stability but also helped to avoid metal sintering and carbon deposition, therefore Ni-Mg PSNTS@silica exhibited an effective and stable performance for DRM.

4. Conclusion

In conclusion, a multicore-shell catalyst was successfully synthesized by silica coating of Ni-Mg PSNTS. Used as catalysts for DRM, Ni-Mg PSNTS suffered from a heavy carbon deposition due to the decomposition of nanotubular structure at high temperature. Ni-Mg PSNTS@silica, which can form multiple small Ni cores supported along nanotubes and encapsulated within one single silica shell after H_2 reduction, was able to stand a reaction temperature as high as 750 °C. Besides, due to the confinement effect conferred by the highly thermal stable mesoporous silica shell, assisted by the interaction between metal and nanotubular support (core@tube confinement), it showed a high and stable activity, while metal sintering and carbon deposition was effectively inhibited. This strategy, typically taking carriers already supporting multiple metal nanoparticles or containing their precursors as the core is believed to be promising and feasible for design and synthesis multicore-shell catalysts for high carbon coking reactions.

Appendix A. Supplementary data

Supplementary data associated with this article can be found, in the online version, at http://dx.doi.org/10.1016/j.apcatb.2016.05.001.

References

[1] D. Pakhare, J. Spivey, Chem. Soc. Rev. 43 (2014) 7813–7837.
[2] M.-S. Fan, A.Z. Abdullah, S. Bhatia, ChemCatChem 1 (2009) 192–208.
[3] U. Y. Kathiraser, E.T. Oemar, Z. Saw, S. Li, Chem. Eng. J. 278 (2015) 62–78.
[4] C.-j. Liu, J. Ye, J. Jiang, Y. Pan, ChemCatChem 3 (2011) 529–541.
[5] S. Kawi, Y. Kathiraser, J. Ni, U. Oemar, Z. Li, E.T. Saw, ChemSusChem 8 (2015) 3556–3575.
[6] M. García-Diéguez, I.S. Pieta, M.C. Herrera, M.A. Larrubia, L.J. Alemany, J. Catal. 270 (2010) 136–145.
[7] D. Li, Y. Nakagawa, K. Tomishige, Appl. Catal. A 408 (2011) 1–24.
[8] T. Xie, L. Shi, J. Zhang, D. Zhang, Chem. Commun. 50 (2014) 7250–7253.
[9] L. Mo, K.K.M. Leong, S. Kawi, Catal. Sci. Technol. 4 (2014) 2107–2114.
[10] K. Sutthiumporn, S. Kawi, Int. J. Hydrogen Energy 36 (2011) 14435–14446.
[11] L. Yao, J. Shi, C. Hu, RSC Adv. 5 (2015) 90168–90177.
[12] H. Wu, G. Pantaleo, V. La Parola, A.M. Venezia, X. Collard, C. Aprile, L.F. Liotta, Appl. Catal. B 156–157 (2014) 350–361.
[13] X.Y. Gao, J. Ashok, S. Widjaja, K. Hidajat, S. Kawi, Appl. Catal. A 503 (2015) 34–42.
[14] L. Mo, E.T. Saw, Y. Du, A. Borgna, M.L. Ang, Y. Kathiraser, Z. Li, W. Thitsartarn, M. Lin, S. Kawi, Int. J. Hydrogen Energy 40 (2015) 13388–13398.
[15] S. Wen, M. Liang, J. Zou, S. Wang, X. Zhu, L. Liu, Z.-j. Wang, J. Mater. Chem. A 3 (2015) 13299–13307.
[16] J. Estephane, S. Aouad, S. Hany, B. El Khoury, C. Gennequin, H. El Zakhem, J. El Nakat, A. Aboukaïs, E. Abi Aad, Int. J. Hydrogen Energy 40 (2015) 9201–9208.
[17] U. Oemar, K. Hidajat, S. Kawi, Int. J. Hydrogen Energy 40 (2015) 12227–12238.
[18] H. Ay, D. Üner, Appl. Catal. B 179 (2015) 128–138.
[19] Y. Kathiraser, W. Thitsartarn, K. Sutthiumporn, S. Kawi, J. Phy. Chem. C 117 (2013) 8120–8130.
[20] T. Odedairo, W. Zhou, J. Chen, Z. Zhu, RSC Adv. 4 (2014) 21306–21312.
[21] K. Sutthiumporn, T. Maneerung, Y. Kathiraser, S. Kawi, Int. J. Hydrogen Energy 37 (2012) 11195–11207.
[22] E.-h. Yang, N.Y. Kim, Y.-s. Noh, S.S. Lim, J.-S. Jung, J.S. Lee, G.H. Hong, D.J. Moon, Int. J. Hydrogen Energy 40 (2015) 11831–11839.
[23] M.A. Lucchini, A. Testino, A. Kambolis, C. Proff, C. Ludwig, Appl. Catal. B 182 (2016) 94–101.
[24] J. Zhang, F. Li, Appl. Catal. B 176–177 (2015) 513–521.
[25] L. Li, S. He, Y. Song, J. Zhao, W. Ji, C.-T. Au, J. Catal. 288 (2012) 54–64.
[26] C. Ding, X. Gao, Y. Han, X. Ma, J. Wang, S. Liu, K. Zhang, J. Energy Chem. 24 (2015) 45–53.
[27] Z. Li, Y. Kathiraser, U. Oemar, S. Kawi, Langmuir 30 (2014) 14694–14705.
[28] Z. Li, Y. Kathiraser, S. Kawi, ChemCatChem 7 (2015) 160–168.
[29] Z. Li, L. Mo, Y. Kathiraser, S. Kawi, ACS Catal. 4 (2014) 1526–1536.
[30] E. Baktash, P. Littlewood, R. Schomäcker, A. Thomas, P.C. Stair, Appl. Catal. B 179 (2015) 122–127.
[31] D.H. Kim, S.Y. Kim, S.W. Han, Y.K. Cho, M.-G. Jeong, E.J. Park, Y.D. Kim, Appl. Catal. A 495 (2015) 184–191.
[32] Z.-Y. Lim, C. Wu, W.G. Wang, K.-L. Choy, H. Yin, J. Mater. Chem. A 4 (2016) 153–159.
[33] S. Li, J. Gong, Chem. Soc. Rev. 43 (2014) 7245–7256.
[34] H.C. Zeng, Acc. Chem. Res. 46 (2013) 226–235.
[35] C. Zhang, W. Zhu, S. Li, G. Wu, X. Ma, X. Wang, J. Gong, Chem. Commun. 49 (2013) 9383–9385.
[36] J.W. Han, C. Kim, J.S. Park, H. Lee, ChemSusChem 7 (2014) 451–456.
[37] X. Du, D. Zhang, R. Gao, L. Huang, L. Shi, J. Zhang, Chem. Commun. 49 (2013) 6770–6772.
[38] S. Tada, M. Yokoyama, R. Kikuchi, T. Haneda, H. Kameyama, J. Phy. Chem. C 117 (2013) 14652–14658.
[39] J. Ashok, Y. Kathiraser, M.L. Ang, S. Kawi, Appl. Catal. B 172–173 (2015) 116–128.
[40] Z. Bian, Z. Li, J. Ashok, S. Kawi, Chem. Commun. 51 (2015) 16324–16326.
[41] G. Zhan, H.C. Zeng, Chem. Mater. 27 (2015) 726–734.
[42] S. Qu, S. Pei, S. Zhang, P. Song, Mater. Lett. 102–103 (2013) 56–58.
[43] Y. Yang, Q. Liang, J. Li, Y. Zhuang, Y. He, B. Bai, X. Wang, Nano Res. 4 (2011) 882–890.
[44] H. Matsune, M. Kishida, J. Catal. 245 (2007) 392–400.

[45] C.M.Y. Yeung, S.C. Tsang, J. Phy. Chem. C 113 (2009) 6074–6087.
[46] E.N. Korytkova, L.N. Pivovarova, Glass Phys. Chem. 36 (2010) 53–60.
[47] S.H. Joo, J.Y. Park, C.-K. Tsung, Y. Yamada, P. Yang, G.A. Somorjai, Nat. Mater. 8 (2009) 126–131.

[48] Y.-g. Chen, K. Tomishige, K. Yokoyama, K. Fujimoto, Appl. Catal. A 165 (1997) 335–347.
[49] X. Pan, X. Bao, Acc. Chem. Res. 44 (2011) 553–562.
[50] H. Tian, X. Li, L. Zeng, J. Gong, ACS Catal. 5 (2015) 4959–4977.